Iranian Journal of Numerical Analysis and Optimization
Vol. 10, No. 1, (2020), pp 81–106
DOI:10.22067/ijnao.v10i1.75129

Research Article

Quasi interpolation of radial basis functions-pseudospectral method for solving nonlinear Klein-Gordon and Sine-Gordon equations

M. Emamjomeh*, S. Abbasbandy and D. Rostamy

Abstract

We propose a new approach for solving nonlinear Klein–Gordon and sine-Gordon equations based on radial basis function-pseudospectral method (RBF-PS). The proposed numerical method is based on quasi-interpolation of radial basis function differentiation matrices for the discretization of spatial derivatives combined with Runge–Kutta time stepping method in order to deal with the temporal part of the problem. The method does not require any linearization technique; in addition, a new technique is introduced to force approximations to satisfy exactly the boundary conditions. The introduced scheme is tested for a number of one- and two-dimensional nonlinear problems. Numerical results and comparisons with reported results in the literature are given to validate the presented method, and the reported results show the applicability and versatility of the proposed method.

AMS(2010): 65N22, 65N35.

Keywords: Meshless method; Pseudospectral method; Radial basis functions; Klein-Gordon equation; sine-Gordon equation; Runge-Kutta fourth order method; Multiquadric quasi-interpolation.

*Corresponding author
Received 6 September 2018; revised 8 October 2019; accepted 15 November 2019
M. Emamjomeh
Department of Applied Mathematics, Faculty of Science, Imam Khomeini International University, Qazvin, Iran. e-mail: emam_me@yahoo.com

S. Abbasbandy
Department of Applied Mathematics, Faculty of Science, Imam Khomeini International University, Qazvin, Iran. e-mail: abbasbandy@ikiu.ac.ir

D. Rostamy
Department of Applied Mathematics, Faculty of Science, Imam Khomeini International University, Qazvin, Iran. e-mail: rostamy@khayam.ut.ac.ir

1 Introduction

The Klein–Gordon equations play an important role in mathematical physics, for example, plasma physics, solid state physics, fluid dynamics, and chemical kinetics [12, 14, 4]. The sine-Gordon equations arise in many different applications and model a soliton wave, which occurs in several physical situations [14]. The theory of plane or cylindrical Josephson junction requires the solutions of sine-Gordon equation in two dimension space [11]. The Josephson junction model, which has various applications in physics, electronics, and so on, consists of two superconducting layers with a tunnel junction between them. This model can be described by the two-dimensional sine-Gordon equation. Here, we consider the following time dependent nonlinear partial differential equation:

$$u_{tt} + \alpha \triangle u + \mathcal{N}(u) = f(x,t), \qquad (x,t) \in \Omega \times \mathbb{R}^+, \tag{1}$$

with initial conditions $u(x,0) = u_0(x)$, $\partial_t u(x,0) = v_0(x)$, and Dirichlet boundary conditions such that (u_0, v_0) belongs the energy space $H^2(\Omega \times \mathbb{R}^+) \times L^2(\Omega \times \mathbb{R}^+)$, where $\Omega \subseteq \mathbb{R}^d, (d = 1, 2)$. We consider the above Cauchy problem associated to the semilinear wave equation, where $\alpha < 0$ is a known constant, $\triangle = \sum_{i=1}^{d} \partial_{x_i}^2$ is the standard space Laplace operator, and $\mathcal{N}$ stands for a nonlinear function. In the well-known sine-Gordon equation, the nonlinear function is given by $\mathcal{N}(u) = \sin(u)$. On the other hand, the higher order Klein–Gordon equation with quadratic and cubic nonlinearity is given by $\mathcal{N}(u) = \beta u + \gamma u^k$ for $k = 2, 3$. Here, we consider the numerical approximation of one- and two-dimensional sine-Gordon equation and the quadratic and cubic nonlinear Klein–Gordon equations. The well-posedness of the Cauchy problem associated with the semi-linear wave equation has been proved in [6, 29]. Many numerical methods such as the finite-difference method, finite element method, spectral method, and so on, have been employed to solve nonlinear Klein–Gordon equations mentioned above[16, 44, 47].

Recently, several numerical methods have been proposed based on radial basis functions (RBFs) in order to solve various types of ordinary and partial differential equations[2, 3, 1, 34, 28, 40, 39, 10, 27, 30, 23, 15, 36, 5]. Usually, RBF methods need to solve the ill-conditioned linear system in order to solve partial differential equations (PDEs). To overcome this difficulty, various methods have been proposed, such as the multiquadric quasi-interpolation (MQQI) method [32]. Here, we will study the numerical solutions of the nonlinear Klein–Gordon and the sine-Gordon equations based on a combination of radial basis functions (RBF) and pseudospectral method MQQI. The differentiation matrices based on MQQI method, are constructed to discretize the spatial derivatives, and Runge–Kutta time stepping method is used to deal with the temporal part of the problem. The method does not need to use any linearization technique. In addition, a new technique is introduced to force approximations to satisfy exactly the boundary conditions. The pre-

sented method is tested for one- and two-dimensional nonlinear problems in order to show its efficiency and accuracy. Numerical results and comparisons with reported results in the literature are given to validate the presented method.

2 Multiquadric Quasi-interpolation

Quasi-interpolation methods are very useful tools in the analysis of scattered data both in theory and in application areas such as the computer science, economy, medicine, and geology. Multiquadric functions were introduced by Hardy [25], and then Franke [18] used them in numerical experiments. Authors in [35, 8, 7, 22, 19, 20, 21] successively proposed a number of quasi-interpolation schemes and discussed their convergence. Useful quasi-interpolation operator $\mathcal{L}_{\mathcal{D}}f$ was proposed by Wu and Schaback [46]. They discussed the convergence and shape preserving properties of this operator. They proved a convergence theorem for interpolated functions $f \in C^2$. Zhang, Liang, and Li [48] proved the convergence of quasi-interpolation operator $\mathcal{L}_{\mathcal{D}}f$ for a wider range of functions.

Assume that there are N points in the bounded interval $\Omega = [a, b]$ as follows:

$$a = x_1 < x_2 < \cdots < x_{N-1} < x_N = b.$$

Let

$$h = \max\{(x_j - x_{j-1}), \quad j = 2, \ldots, N\}.$$

In [46], the MQ quasi-interpolation operator $\mathcal{L}_{\mathcal{D}}$ has been defined:

$$(\mathcal{L}_{\mathcal{D}}f)(x) = \sum_{j=1}^{N} f_j \phi_j(x), \tag{2}$$

where

$$\begin{cases} \phi_1(x) = \frac{1}{2} + \frac{\psi_2(x)-(x-x_1)}{2(x_2-x_1)}, \\ \phi_2(x) = \frac{\psi_3(x)-\psi_2(x)}{2(x_3-x_2)} - \frac{\psi_2(x)-(x-x_1)}{2(x_2-x_1)}, \\ \phi_j(x) = \frac{\psi_{j+1}(x)-\psi_j(x)}{2(x_{j+1}-x_j)} - \frac{\psi_j(x)-\psi_{j-1}(x)}{2(x_j-x_{j-1})}, \quad j = 3, \ldots, N-2, \\ \phi_{N-1}(x) = \frac{(x-x)-\psi_{N-1}(x)}{2(x_N-x_{N-1})} - \frac{\psi_{N-1}(x)-\psi_{N-2}(x)}{2(x_{N-1}-x_{N-2})}, \\ \phi_N(x) = \frac{1}{2} + \frac{\psi_{N-1}(x)-(x_N-x)}{2(x_N-x_{N-1})}, \end{cases} \tag{3}$$

and $\psi_j(x)$ are the multiquadrics RBF (MQ-RBF) as follows:

$$\psi_j(x) = \sqrt{c^2 + (x - x_j)^2}, \quad j = 2, \ldots, N-1. \tag{4}$$

The univariate MQ quasi-interpolation scheme can be extended into higher dimensions simply by applying it to each of the coordinates independently. In this paper, the scheme of dimension-splitting MQ (DS-MQ) proposed in [31, 33] for approximation of $f(x), x = (\xi, \eta) \in \mathbb{R}^2$ is used, and this function will be approximated as follows:

$$f(x) = f(\xi, \eta) \simeq (\mathcal{L}_{\mathcal{D}} f)(\xi, \eta) = \sum_{i=1}^{N_1} \sum_{j=1}^{N_2} f_{ij} \phi_i(\xi) \phi_j(\eta) = \sum_{k=1}^{N} f_k \Phi_k(x), \quad (5)$$

where $N = N_1 \times N_2$ is the number of data points, f_{ij} is the value of f at the intersection of the ith horizontal grid line and the jth vertical grid line, and $\phi_i(\xi)$ and $\phi_j(\eta)$ are defined by (3). Functions $\Phi_k(x) = \Phi_k(\xi, \eta)$ in (5) are obtained by product of $\phi_i(\xi)$ into $\phi_j(\eta)$ and $f_k = f(x_k) = f(\xi_k, \eta_k), k = 1, \ldots, N$.

3 Derivative approximation by the RBF-PS method

The differentiation matrices have proved to be a very useful tool in the numerical solutions of differential equations. In this work, differentiation matrices are derived from the radial-basis pseudospectral (PS) method. PS methods are numerical methods with high precision, which use polynomials as basis functions. Chebyshev pseudospectral method (CHEB-PS) is one type of them, which uses Chebyshev polynomials as basis functions. An important attribute of PS methods is that approximate solutions are obtained on a discrete set of grid points $x_j, j = 1, \ldots, N$ and in solving differential equations with PS methods, we will need to represent values of derivatives of u at grid points. The radial basis function-pseudospectral (RBF-PS) method involves the common approach of all weighted residual methods, that is, approximating the field using a combination of some pre-defined functions termed as shape functions and some unknown coefficients, which are determined depending upon the governing equation of the problem. In the RBF-PS method, shape functions are computed by using RBFs. Fasshauer [17] proposed the application of infinitely smooth RBFs in pseudospectral formulation and interpreted the combined approach as a meshless RBF-PS method.

For a given set of centers $x_j, j = 1, \ldots, N$, an MQQI approach of the solution $u(x, t)$ of a PDE is given by

$$u_N(x, t) = \sum_{j=1}^{N} \xi_j(t) \phi_j(x), \quad (6)$$

where $\phi_j(x), j = 1, \ldots, N$ are defined by (3) for one-dimensional and $\Phi_j(x, y)$ are defined by (5) for two-dimensional.

Now, if we evaluate the approximate solution $u_N(x,t)$ at the grid points $x_i, i = 1,\ldots,N$, and at fixed time t, then we get

$$u_N(x_i,t) = \sum_{j=1}^{N} \xi_j(t)\phi_j(x_i), \qquad i = 1,\ldots,N. \tag{7}$$

Which can be written in the following matrix form:

$$\boldsymbol{u}(t) = A\boldsymbol{\xi}(t), \tag{8}$$

where

$$\boldsymbol{\xi}(t) = [\xi_1(t),\ldots,\xi_N(t)]^T,$$

$$A_{i,j} = \phi_j(x_i), \quad i,j = 1,\ldots,N,$$

and

$$\boldsymbol{u}(t) = [u_N(x_1,t),\ldots,u_N(x_N,t)]^T.$$

Suppose that $\mathfrak{L}$ is a linear differential operator relative to the x. By applying the operator $\mathfrak{L}$ to expansion (6) and use linearity of $\mathfrak{L}$, we have

$$\mathfrak{L}u_N(x,t) = \sum_{j=1}^{N} \xi_j(t)\mathfrak{L}\phi_j(x). \tag{9}$$

If we again evaluate (9) at the grid points $x_i, i = 1,\ldots,N$, and using matrix notation, then we get

$$\mathfrak{L}\boldsymbol{u} = A_{\mathfrak{L}}\boldsymbol{\xi}(t), \tag{10}$$

where $\boldsymbol{\xi}(t)$ is as above, $\mathfrak{L}\boldsymbol{u} = [\mathfrak{L}u_N(x_1,t),\ldots,\mathfrak{L}u_N(x_N,t)]^T$, and the matrix $A_{\mathfrak{L}}$ has entries $\mathfrak{L}\phi_j(x_i)$. Then, we use (8) to solve the coefficient vectors $\boldsymbol{\xi}(t) = A^{-1}\boldsymbol{u}$, and then (10) yields

$$\mathfrak{L}\boldsymbol{u} = A_{\mathfrak{L}}A^{-1}\boldsymbol{u}, \tag{11}$$

so that the operational matrix $\mathfrak{L}$ corresponding to linear operator $\mathfrak{L}$ is given by

$$\mathfrak{L} = A_{\mathfrak{L}}A^{-1}. \tag{12}$$

In order to obtain the differentiation matrix $\mathfrak{L}$, we need to ensure invertibility of the evaluation matrix A. This generally depends both on the basis functions chosen as well as the location of the grid points x_i. For positive definite RBFs, it is well known that the evaluation matrix is invertible for any set of distinct grid points [45, 38]. For positive semidefinite radial basis functions, it is possible to construct a counterexample that leads to a singular matrix, though, such counterexamples are found rather seldom and with difficulty [45].

Remark. In the special case if $\mathfrak{L} = \triangle$, then

$$\triangle \boldsymbol{u} = \mathfrak{D}_{\mathfrak{L}}.\boldsymbol{u}, \tag{13}$$

where

$$\mathfrak{D}_{\mathfrak{L}} = A_{\mathfrak{L}} A^{-1}, \tag{14}$$

such that in one-dimensional $\triangle = \frac{d^2}{dx^2}$ and

$$(A_{\mathfrak{L}})_{ij} = (\frac{d^2\phi_j(x)}{dx^2})|_{x=x_i}. \tag{15}$$

Also, in two-dimensional, we have $\triangle = \frac{\partial^2}{\partial x^2} + \frac{\partial^2}{\partial y^2}$ and

$$(A_{\mathfrak{L}})_{ij} = (\frac{\partial^2\Phi_j(x,y)}{\partial x^2} + \frac{\partial^2\Phi_j(x,y)}{\partial y^2})|_{(x,y)=(x_i,y_i)}. \tag{16}$$

4 New numerical scheme

Now, we present the numerical scheme for solving the Klein–Gordon equation (17)–(20) by using the MQ quasi-interpolation operator $\mathcal{L}_{\mathcal{D}}$. In our scheme, the collocation scheme is applied at grid points x_i, $i = 1, \ldots, N$. Then, the highest order derivatives (second order in this paper) of the solution function are approximated by the differentiation matrix. Then, the fourth order Runge–Kutta method is employed to the approximate solution of the first order ordinary differential equations (ODEs) system.

We first discuss our scheme for the nonlinear Klein–Gordon equation with quadratic and cubic nonlinearity in one-dimensional and two-dimensional space, and finally, we apply the numerical algorithm to solve the sine-Gordon equation. In the following, we consider the following nonlinear Klein–Gordon equation:

$$u_{tt}(x,t) + \alpha \triangle u(x,t) + \beta u(x,t) + \gamma(u(x,t))^k = f(x,t), \tag{17}$$

for $\alpha < 0$ with the initial conditions:

$$u(x,0) = u_0(x), \qquad x \in \Omega, \tag{18}$$

$$u_t(x,0) = v_0(x), \qquad x \in \Omega, \tag{19}$$

and Dirichlet boundary conditions:

$$u(x,t) = g(t), \qquad t \in (0,T], \qquad x \in \partial\Omega, \tag{20}$$

where Ω is a bounded domain in $\mathbb{R}^d (d = 1, 2)$ and $\partial\Omega$ is the boundary of Ω. We transform the problem (17)–(20) into a system of coupled first order equation in time given by

$$\begin{cases} u_t(x,t) = v(x,t), \\ v_t(x,t) = -\alpha \triangle u(x,t) - \beta u - \gamma u^k + f(x,t), \end{cases} \tag{21}$$

with the initial conditions

$$u(x,0) = u_0(x), \qquad x \in \Omega, \tag{22}$$

$$v(x,0) = v_0(x), \qquad x \in \Omega, \tag{23}$$

and boundary condition

$$u(x,t) = g(t), \qquad t \in (0,T], \qquad x \in \partial\Omega. \tag{24}$$

In the following, we give the structure of this scheme.

4.1 Step one: *Semidiscretization in space*

If we evaluate the MQQI approach of $u(x,t)$ and $v(x,t)$ at grid points x_i, $i = 1, \ldots, N$ and at fixed time t, then we get

$$u_N(x_i,t) = \sum_{j=1}^{N} \xi_j(t)\phi_j(x_i), \qquad i = 1, \ldots, N, \tag{25}$$

$$v_N(x_i,t) = \sum_{j=1}^{N} \beta_j(t)\phi_j(x_i), \qquad i = 1, \ldots, N. \tag{26}$$

If we evaluate (21) at each node $x_i, i = 1, \ldots, N$, and use (13) to approximate $\triangle u(x_i,t)$ and equations display in a matrix form, then we get

$$\begin{cases} \frac{d\boldsymbol{U}}{dt} = \boldsymbol{V}(X,t), \\ \frac{d\boldsymbol{V}}{dt} = -\alpha \mathfrak{D}_{\mathfrak{L}}.\boldsymbol{U}(X,t) - \beta \boldsymbol{U}(X,t) - \gamma \boldsymbol{U}^k(X,t) + \boldsymbol{f}(X,t), \end{cases} \tag{27}$$

where $X = [x_1, x_2, \ldots, x_N]^T$, $\boldsymbol{U}(X,t) = [\boldsymbol{u}_1(t), \ldots, \boldsymbol{u}_N(t)]^T$, $\boldsymbol{V}(X,t) = [\boldsymbol{v}_1(t), \ldots, \boldsymbol{v}_N(t)]^T$ and $\boldsymbol{f}(X,t) = [f(x_1,t), \ldots, f(x_N,t)]^T$, in which $\boldsymbol{u}_i(t)$ and $\boldsymbol{v}_i(t)$ are approximations of $u(x_i,t)$ and $v(x_i,t), i = 1, \ldots, N$ and $\mathfrak{D}_{\mathfrak{L}}$ is the differentiation matrix defined in (14) and unchanged in time steps. In a more compact form, (27) can be written as

$$\begin{cases} \frac{d\boldsymbol{U}}{dt} = \boldsymbol{F}_1(t, \boldsymbol{U}, \boldsymbol{V}), \\ \frac{d\boldsymbol{V}}{dt} = \boldsymbol{F}_2(t, \boldsymbol{U}, \boldsymbol{V}), \end{cases} \tag{28}$$

with initial values

$$\begin{cases} \boldsymbol{U}(0) = u(X, 0) = u_0(X), \\ \boldsymbol{V}(0) = u_t(x, 0) = v_0(X), \end{cases} \tag{29}$$

where

$$\begin{cases} \boldsymbol{F}_1(t, \boldsymbol{U}, \boldsymbol{V}) = \boldsymbol{V}(X, t), \\ \boldsymbol{F}_2(t, \boldsymbol{U}, \boldsymbol{V}) = -\alpha \mathfrak{D}_{\mathfrak{L}}.\boldsymbol{U}(X, t) - \beta \boldsymbol{U}(X, t) - \gamma \boldsymbol{U}^k(X, t) + \boldsymbol{f}(X, t). \end{cases} \tag{30}$$

Remark. In the above, the vector $\boldsymbol{U}^k$ equals $\boldsymbol{U} \bigotimes \boldsymbol{U} \bigotimes \cdots \bigotimes \boldsymbol{U}$ and the symbol $\bigotimes$ denotes the component by component multiplication of two vectors. We can easily repeat the above step for nonlinear sine-Gordon equation by replacing the vector $\boldsymbol{U}^k$ with the vector $sin(\boldsymbol{U})$.

4.2 Step two: *Time discretization*

In this section, we apply fourth-order Runge–Kutta scheme to solve the system of ODEs (28).
Let

$$\boldsymbol{U}^{(m)} = \boldsymbol{U}_N^{(m)} = (u_N(x_i, t_m))_{i=1}^N = (\sum_{j=1}^N \xi_j^{(m)} \phi_j(x_i))_{i=1}^N$$

and let

$$\boldsymbol{V}^{(m)} = \boldsymbol{V}_N^{(m)} = (v_N(x_i, t_m))_{i=1}^N = (\sum_{j=1}^N \beta_j^{(m)} \phi_j(x_i))_{i=1}^N$$

where $\xi_j^{(m)} = \xi_j(t_m)$, $\beta_j^{(m)} = \beta_j(t_m)$, and $t_m = mdt$.
Then, from (28) and fourth-order Runge–Kutta method, we have

$$\begin{cases} \boldsymbol{U}^{(m+1)} = \boldsymbol{U}^{(m)} + \frac{1}{6}(\boldsymbol{K}_{1,1} + 2\boldsymbol{K}_{2,1} + 2\boldsymbol{K}_{3,1} + \boldsymbol{K}_{4,1}), \\ \boldsymbol{V}^{(m+1)} = \boldsymbol{V}^{(m)} + \frac{1}{6}(\boldsymbol{K}_{1,2} + 2\boldsymbol{K}_{2,2} + 2\boldsymbol{K}_{3,2} + \boldsymbol{K}_{4,2}), \end{cases} \tag{31}$$

where
$\boldsymbol{K}_{1,1} = dt\boldsymbol{F}_1(t^{(m)}, \boldsymbol{U}^{(m)}, \boldsymbol{V}^{(m)})$,
$\boldsymbol{K}_{2,1} = dt\boldsymbol{F}_1(t^{(m)} + \frac{dt}{2}, \boldsymbol{U}^{(m)} + \frac{1}{2}\boldsymbol{K}_{1,1}, \boldsymbol{V}^{(m)} + \frac{1}{2}\boldsymbol{K}_{1,2})$,
$\boldsymbol{K}_{3,1} = dt\boldsymbol{F}_1(t^{(m)} + \frac{dt}{2}, \boldsymbol{U}^{(m)} + \frac{1}{2}\boldsymbol{K}_{2,1}, \boldsymbol{V}^{(m)} + \frac{1}{2}\boldsymbol{K}_{2,2})$,

$\boldsymbol{K}_{4,1} = dt\boldsymbol{F}_1(t^{(m)} + dt, \boldsymbol{U}^{(m)} + \boldsymbol{K}_{3,1}, \boldsymbol{V}^{(m)} + \boldsymbol{K}_{3,2})$,
and $\boldsymbol{K}_{i,2}$ is similar to $\boldsymbol{K}_{i,1}$, $i = 1, \ldots, 4$.

4.3 Step three: *Apply the boundary conditions*

The other half of the technique is the imposition of the boundary conditions. There are two basic ways of dealing with boundary conditions. The first is to use the basis functions that satisfy the boundary condition exactly. This is possible when the domain is regular and the boundary conditions are simple such as homogeneous or periodic boundary conditions. In other cases, the second approach may be used, where some of the additional equations are used to enforce the boundary conditions. Here, we use the algorithm given in [17, 42] with some modifications. The boundary conditions will be imposed by modifying vector $\boldsymbol{U}^{(m+1)}$ in (31). Replace those components of $\boldsymbol{U}^{(m+1)}$ corresponding to grid points at boundary domain with the exact boundary conditions at time level $(m+1)dt$. So we modified $\boldsymbol{U}^{(m+1)}$ in (31) with the following:

$$\boldsymbol{U}^{(m+1)} = I_\partial \boldsymbol{U}^{(m+1)} + \boldsymbol{U}_\partial^{(m+1)}, \tag{32}$$

where I_∂ is the matrix resulting from the replacement the rows corresponding to the boundary points with zero in the identity matrix and $\boldsymbol{U}_\partial^{(m+1)}$ is the vector resulting from the replacement the components corresponding to the boundary points with the exact boundary conditions in the zero vector.

5 Numerical examples

In this section, several numerical examples are given to show the efficiency of our proposed method for approximating the solution of nonlinear Klein–Gordon equation and Sine–Gordon equation by comparing with other methods.

we first consider nonlinear Klein–Gordon equation (17)–(20), and finally, this scheme is applied for Sine–Gordon equation in both one-dimensional and two-dimensional cases.

We use the univariate and two-dimensional MQQI $\mathcal{L}_\mathcal{D}$ directly to approximate functions u^m and $\triangle u^m$. For all computations in this paper, we choose fixed values of the shape parameters of the kernel functions, and the relationship between the shape parameter and the error norm is shown in the examples. In order to test the performance of the method and accuracy of approximate solutions, L_∞, L_2, and root-mean-square (RMS) errors will be used, which are defined as

$$L_\infty \ \ error = \max_{1\le j\le N} |u(x_j,t_m) - u_N(x_j,t_m)|,$$

$$L_2 \ \ error = \sqrt{h\sum_{j=1}^{N}(u(x_j,t_m) - u_N(x_j,t_m))^2},$$

$$RMS \ \ error = \sqrt{\frac{\sum_{j=1}^{N}(u(x_j,t_m) - u_N(x_j,t_m))^2}{N}},$$

for $0 \le t_m \le T$, where u and u_N denote the exact and numerical solutions of the problem, respectively.

5.1 Klein–Gordon equation

In the case of one-dimensional nonlinear Klein–Gordon equations, we compare our numerical results with analytical solutions, solutions in [13], and those in [37]. Dehghan and Shokri [13] used thin plate splines (TPS), RBF collocation method. To approximate the solution function and second order derivative of the solution, Sarboland and Aminataei [37] used the integrated form of MQ quasi-interpolation scheme(IMQQI). They showed that their scheme requires fewer nodes to attain accuracy of TPS method, and in this work, it is shown that for presented examples, the errors in our method are better than those in [37]. In two-dimensional Klein–Gordon equations, we compare our numerical solution with the exact solutions, approximate solution in [41], and we show that the numerical results are in good agreement with the exact solution and that our scheme requires fewer nodes to attain accuracy of MK-MLPG method.

Example 1. Consider problem (17)–(20) with interval $x \in [-1,1]$, $\alpha = -1, \beta = 0, \gamma = 1$, and $k = 2$. The initial conditions are given by

$$\begin{cases} u(x,0) = x, \\ u_t(x,0) = 0, \end{cases}$$

and $f(x,t) = -x\cos t + x^2\cos t$ in the interval $-1 \le x \le 1$. The exact solution is given by

$$u(x,t) = x\cos t. \tag{33}$$

The Dirichlet boundary conditions are extracted from the exact solution easily.

Table 1 presents L_∞ errors, L_2 errors, and RMS errors in Example 1. The results are obtained by using $N = 10$ grid points, $dt = 0.001$, and $c = 0.121$. We compare our results with the reported results in [37]. As can be seen from the tables, the numerical results are in good agreement with the exact solu-

Table 1: Error norms of Example 1 at different times T using $N = 10$ grid points, $dt = 0.001$, and $c = 0.121$

T	L_∞	L_2	RMS	L_∞[37]	L_2[37]	RMS[37]
1	2.19755×10^{-14}	2.1570×10^{-14}	1.44696×10^{-14}	1.2590×10^{-5}	2.0694×10^{-5}	6.2397×10^{-6}
3	1.30590×10^{-14}	1.23829×10^{-14}	8.30668×10^{-15}	1.5428×10^{-5}	3.7065×10^{-5}	1.1175×10^{-6}
5	2.72352×10^{-14}	2.57676×10^{-14}	1.72854×10^{-14}	3.3625×10^{-5}	6.9684×10^{-5}	2.1010×10^{-5}
7	2.08028×10^{-14}	2.03321×10^{-14}	1.36392×10^{-14}	3.7412×10^{-5}	8.1943×10^{-5}	2.4706×10^{-5}

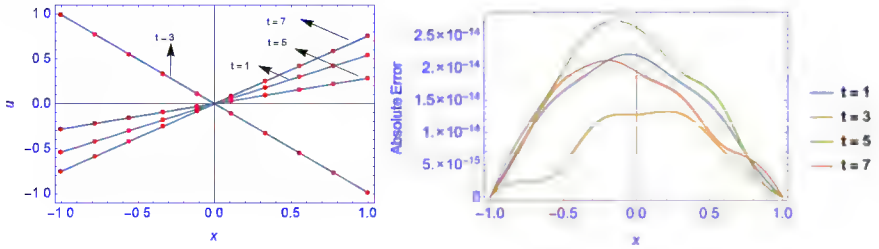

Figure 1: Numerical and exact solutions of Example 1 (left) and error of method (right) with $N = 10$, $dt = 0.001$

tion.The graphs of the numerical and analytical solutions for different times with $dx = 0.2, dt = 0.001$ in the interval $-1 \leq x \leq 1$ and using MQQI-PS (with $c = 0.121$) are shown in Figure 1.

Example 2. In this example, we consider the one-dimensional nonlinear hyperbolic Klein Gordon equation (17) in the interval $0 \leq x \leq 1$, $\alpha = -1, \beta = 0, \gamma = 1, andk = 2$. The initial conditions are given by

$$\begin{cases} u(x,0) = 0, \\ u_t(x,0) = 0, \end{cases}$$

and $f(x,t) = 6xt(x^2 - t^2) + x^6t^6$ in the interval $0 \leq x \leq 1$. The exact solution of this example is

$$u(x,t) = x^3t^3. \tag{34}$$

The Dirichlet boundary conditions are extracted from the exact solution easily.

Table 2: Error norms of Example 2 at different times T using $N = 20$ grid points, $dt = 0.001$, MQQI-PS and $c = 0.381$

	MQQI - PS			*IMQQI*		
T	L_∞	L_2	RMS	L_∞[37]	L_2[37]	RMS[37]
1	4.03996×10^{-6}	1.73964×10^{-6}	1.69559×10^{-6}	7.7958×10^{-6}	3.4694×10^{-5}	4.8581×10^{-6}
2	1.76028×10^{-5}	7.79986×10^{-6}	7.60237×10^{-6}	1.2307×10^{-4}	5.5475×10^{-4}	7.7680×10^{-5}
3	1.89709×10^{-4}	7.44319×10^{-5}	7.25472×10^{-5}	5.3019×10^{-4}	2.4618×10^{-3}	2.4473×10^{-4}
4	5.75087×10^{-4}	2.18034×10^{-4}	2.12514×10^{-4}	1.8601×10^{-3}	2.4618×10^{-3}	9.7029×10^{-4}
5	1.5485×10^{-3}	6.47638×10^{-4}	6.31239×10^{-4}	3.5192×10^{-3}	1.3585×10^{-2}	1.9022×10^{-3}

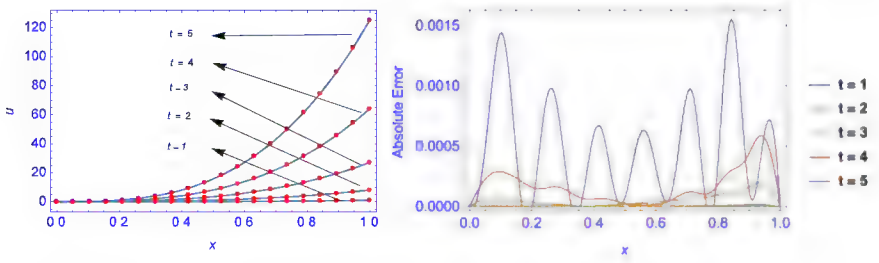

Figure 2: Numerical and exact solutions (left)of Example 2 and error of method (right) with $N = 20$, $dt = 0.001$ at $T = 1, 2, \cdots, 5$

Table 3: Error norms of Example 3 at different times T using $N = 50$ grid points, $\delta t = 0.001$, MQQI-PS, and $c = 0.181$

T	L_∞	L_2	RMS	L_∞[37]	L_2[37]	RMS [37]
1	2.83572×10^{-4}	1.59049×10^{-4}	1.11334×10^{-4}	4.2672×10^{-5}	2.8456×10^{-4}	2.0242×10^{-5}
2	7.81595×10^{-4}	3.84643×10^{-4}	2.6925×10^{-4}	4.9397×10^{-4}	2.6266×10^{-3}	1.8577×10^{-4}
3	6.78361×10^{-4}	1.61686×10^{-4}	1.1318×10^{-4}	2.0380×10^{-3}	9.5859×10^{-3}	6.7016×10^{-4}
4	1.09944×10^{-4}	7.14267×10^{-5}	4.99987×10^{-5}	6.4162×10^{-3}	2.3457×10^{-2}	1.8844×10^{-3}
5	3.22279×10^{-4}	1.60303×10^{-4}	1.12212×10^{-4}	1.7941×10^{-2}	7.4214×10^{-2}	5.2391×10^{-3}

Table 2 presents L_∞ errors, L_2 errors, and RMS errors in Example 2. The results are obtained by using $N = 20$ grid points, $dt = 0.001$, MQQI-PS, and $c = 0.381$. We compare our results with the reported results in [37]. As can be seen from the tables, the numerical results are in good agreement with the exact solution. Figure 2 compares numerical and exact solutions of Example 2 with $N = 20$ grid points and $dt = 0.001$ at different times T.

Example 3. In this example, we consider the one-dimensional nonlinear hyperbolic Klein–Gordon equation (17) in $x \in [-1, 1]$, with $\alpha = -1, \beta = 1, \gamma = 1$and $k = 3$. The initial conditions are given by

$$\begin{cases} u(x,0) = x^2 \cosh x, -1 \le x \le 1, \\ u_t(x,0) = x^2 \sinh x, -1 \le x \le 1, \end{cases}$$

and the right-hand side function is
$f(x,t) = (x^2 - 2)\cosh(x+t) - 4x\sinh(x+t) + x^6 \cosh^3(x+t)$.
The exact solution is given as

$$u(x,t) = x^2 \cosh(x+t). \tag{35}$$

The Dirichlet boundary conditions are extracted from the exact solution easily.

Table 3 presents L_∞ errors, L_2 errors, and RMS errors in Example 3. The results are obtained by using $N = 50$ grid points, $dt = 0.001$, MQQI-PS, and $c = 0.181$. We compare our results with the reported results in [37]. As can be seen from the tables, the numerical results are in good agreement with

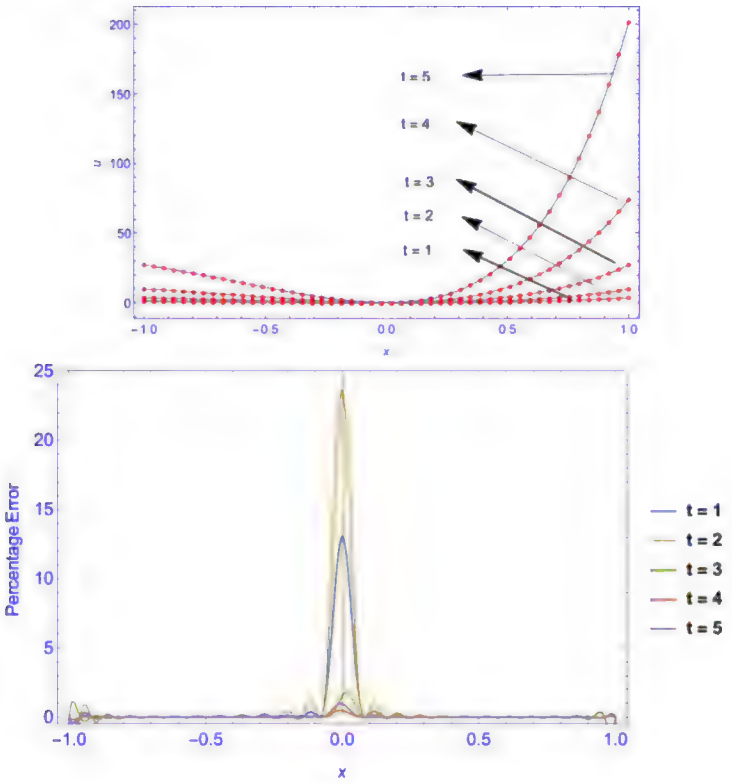

Figure 3: Numerical and exact solutions of Example 3 and error of method with $N = 50$, $dt = 0.001$

the exact solution. Figure 3 compares the numerical and exact solutions of Example 3 with $N = 50$ grid points and $dt = 0.001$ at different times T.

Example 4. In this example, we consider the one dimensional nonlinear hyperbolic Klein Gordon equation (17) in $x \in [0, 1]$, with $\alpha = -2.5, \beta = 1, \gamma = 1.5$, and $k = 3$ and $f(x, t) = 0$. The exact solution is given by:

$$u(x, t) = B \tan(K(x + Ct)), \tag{36}$$

where $B = \sqrt{\frac{\beta}{\gamma}}$, $K = \sqrt{\frac{-\beta}{2(\alpha+C^2)}}$.
The initial and boundary conditions are extracted from the exact solution easily.

Table 4 presents L_∞ errors, L_2 errors, and RMS errors in Example 4 with $C = 0.05$. The results are obtained by using $N = 20$ grid points, $dt = 0.001$, MQQI-PS, and $c = 2.2$. We compare our results with the reported results in [37]. As can be seen from the tables, the numerical results are in good agree-

Table 4: Error norms of Example 4 with $C = 0.05$ at different times T using $N = 20$ grid points, $dt = 0.001$, $\alpha = -2$, $\beta = 1$, $\gamma = 1.5$, MQQI-PS method and MQQI shape parameter $c = 2.2$

T	L_∞	L_2	RMS	L_∞[37]	L_2[37]	RMS [37]
1	8.10099×10^{-7}	4.07215×10^{-7}	3.96904×10^{-7}	2.1781×10^{-7}	1.2850×10^{-6}	1.2787×10^{-7}
2	2.34139×10^{-6}	1.21136×10^{-6}	1.18068×10^{-6}	3.0648×10^{-7}	1.4099×10^{-6}	1.3980×10^{-7}
3	2.77812×10^{-6}	1.5571×10^{-6}	1.51767×10^{-6}	3.7008×10^{-7}	1.3144×10^{-6}	1.7004×10^{-7}
4	2.63626×10^{-6}	1.21796×10^{-6}	1.18712×10^{-6}	3.4230×10^{-7}	2.0012×10^{-6}	1.2002×10^{-7}

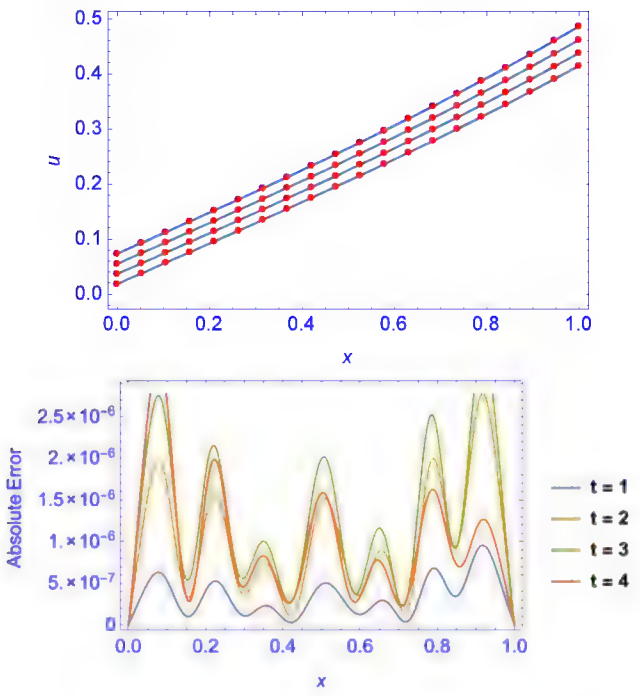

Figure 4: Numerical and exact solutions of Example 4 and error of method with C=0.05, $N = 20$ and $dt = 0.001$ at different times T

ment with the exact solution. Figure 4 compares the numerical and exact solutions of Example 4 with $N = 20$ grid points and $dt = 0.001$ at different times T.

Table 5 presents L_∞ errors, L_2 errors, and RMS errors in Example 4 with $C = 0.5$. The results are obtained by using $N = 50$ grid points, $dt = 0.001$, MQQI-PS method and $c = 0.97$. We compare our results with the reported results in [37]. As can be seen from the tables, the numerical results are in good agreement with the exact solution. Figure 5 compares the numerical and exact solutions of Example 4 with $C = 0.5$, $N = 50$ grid points and $dt = 0.001$ at different times T.

Table 5: Error norms of Example 4 with $C = 0.5$ at different times T using $N = 50$ grid points, $dt = 0.001$, $\alpha = -2$, $\beta = 1$, $\gamma = 1.5$, MQQI-PS method and MQQI shape parameter $c = 0.97$

T	L_∞	L_2	RMS	L_∞[37]	L_2[37]	RMS [37]
1	1.34058×10^{-6}	3.6230×10^{-7}	7.95305×10^{-7}	5.2134×10^{-6}	4.0608×10^{-5}	4.0392×10^{-6}
2	5.28169×10^{-6}	1.462×10^{-6}	1.92792×10^{-6}	2.1805×10^{-5}	1.5588×10^{-4}	1.5505×10^{-5}
3	2.54257×10^{-5}	5.6233×10^{-6}	4.46219×10^{-6}	9.0113×10^{-5}	6.3231×10^{-4}	6.5903×10^{-5}
4	1.32595×10^{-3}	2.53105×10^{-4}	9.82629×10^{-5}	8.2372×10^{-4}	5.3386×10^{-3}	5.3219×10^{-4}

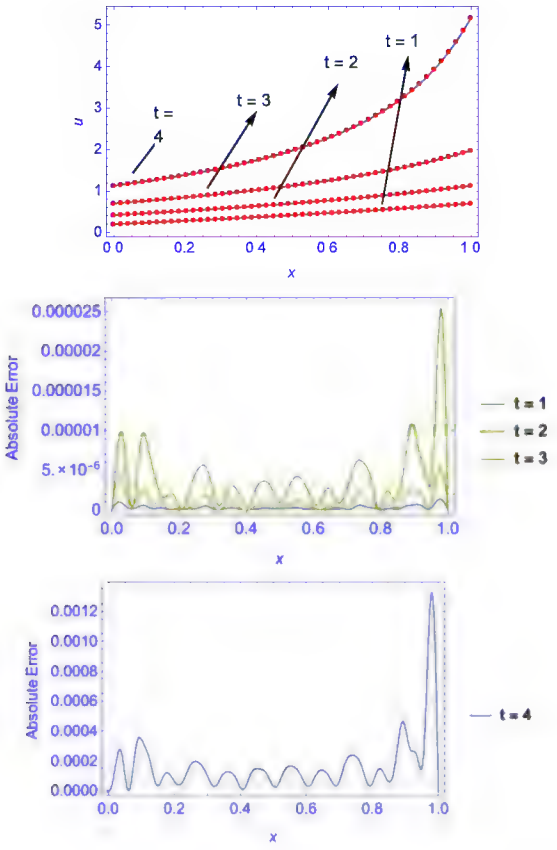

Figure 5: Numerical and exact solutions of Example 4 and error of method with C=0.5, $N = 50$ and $dt = 0.001$ at different times T

Example 5. Let us consider the following two-dimensional nonlinear hyperbolic Klein Gordon equation (17) in $(x, y) \in [0, \pi] \times [0, \pi]$, with $\alpha = -1, \beta = -2, \gamma = 1$, and $k = 2$. The exact solution of this example is

$$u(x, y, t) = \sin(x) \sin(y) \cosh(t), \tag{37}$$

Table 6: Error norms of Example 5 at different times T using $N = 10 \times 10$ uniform grid points, $dt = 0.01$, $\alpha = -1$, $\beta = -2$, $\gamma = 1$, $k = 2$, MQQI-PS method and MQQI shape parameter $c = 4.15$

	$MQQI - PS$	$(N = 10 \times 10)$		$MK - MLPG$	$(N = 33 \times 33)$	
T	L_∞	L_2	RMS	L_∞[41]	L_2[41]	RMS [41]
1	2.32242×10^{-6}	1.4976×10^{-6}	8.40697×10^{-7}	1.04×10^{-3}	1.28×10^{-2}	3.87×10^{-4}
2	3.88411×10^{-6}	2.65018×10^{-6}	1.48771×10^{-6}	1.23×10^{-2}	1.86×10^{-1}	5.64×10^{-3}
3	4.19091×10^{-6}	3.26018×10^{-6}	1.83014×10^{-6}	4.35×10^{-2}	7.52×10^{-1}	2.28×10^{-2}
4	6.10456×10^{-6}	4.66624×10^{-6}	2.61945×10^{-6}	1.20×10^{-1}	2.07×10^{0}	6.27×10^{-2}
5	9.83839×10^{-6}	6.92622×10^{-6}	3.88811×10^{-6}	3.25×10^{-1}	5.77×10^{0}	1.75×10^{-1}

the initial and Dirichlet boundary conditions are extracted from the exact solution easily.

Table 6 presents L_∞ errors, L_2 errors, and RMS errors in Example 5. The

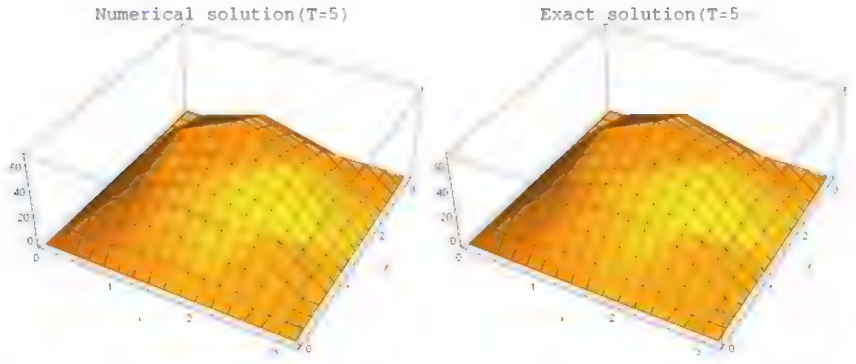

Figure 6: Numerical and exact solution of Example 5 with $N = 10 \times 10$, $dt = 0.01$, $\alpha = -1$, $\beta = -2$, $\gamma = 1$, $k = 2$, and MQQI shape parameter $c = 4.15$ at time t=5

results are obtained by using $N = 10 \times 10$ grid points, $dt = 0.01$, MQQI-PS method, and MQQI shape parameter $c = 4.15$. We compare our results with the reported results in [41]. As can be seen from the tables, the numerical results are in good agreement with the exact solution. Figure 6 compares the numerical and exact solutions of Example 5 with $N = 10 \times 10$ grid points and $dt = 0.01$ at $t = 5$.The contour plot of the absolute error norm for the MQQI-PS method in Example 5 is portrayed in Figure 7. The MQQI shape parameter c versus L_∞ is shown in Figure 8 when $t = 5$, $dt = 0.01$, and $N = 10 \times 10$, corresponding to Example 5.

Table 7 presents comparisons of L_∞ errors, L_2 errors, and RMS errors for the MQ-PS method and MQQI-PS method in Example 5. The results are obtained by using $N = 25 \times 25$ grid points, $dt = 0.01$, MQ-RBF-PS method with shape parameter $c = 0.37$ and MQQI-PS method with shape parameter $c = 4.6$. As can be seen from the tables, the numerical results from MQ-PS and MQQI-PS are in good agreement with the exact solution. The contour

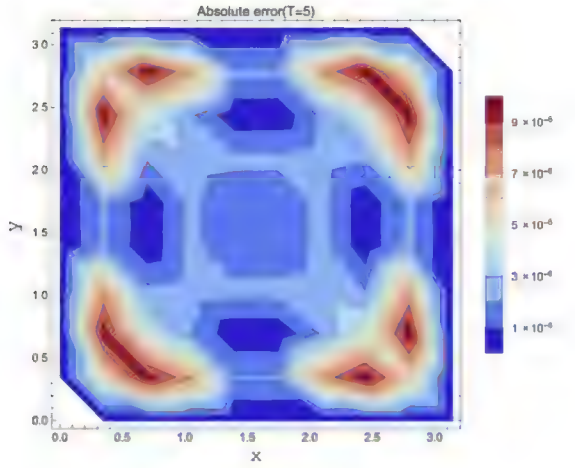

Figure 7: The contour plot of the absolute error norm for the MQQI-PS method in Example 5 with $N = 10 \times 10$, $dt = 0.01$ and MQQI shape parameter $c = 4.15$ at time t=5

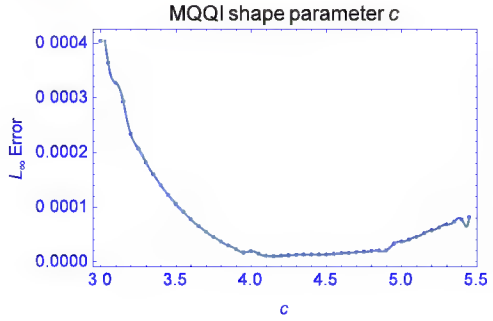

Figure 8: The plot of L_∞ error norm against MQQI-Ps(c) in Example 5 with $N = 10 \times 10$, $dt = 0.01$ and MQQI shape parameter $c = 4.15$ at time t=5

plot of the absolute error norm for the MQ-PS method and MQQI-PS method in Example 5 are compared in Figure 9 by using $N = 25 \times 25$ grid points.

5.2 Sine-Gordon equation

Consider the hyperbolic Klein Gordon equation (1) with nonlinear term $\mathcal{N}(u) = \sin(u)$. In this section, we consider Sine-Gordon equations of the form

$$u_{tt}(x,t) + \alpha \triangle u = -\sin(u). \tag{38}$$

With the initial conditions

Table 7: Compare error of MQ-PS method and MQQI-PS method for Example 5 with $\alpha = -1$, $\beta = -2$, $\gamma = 1$, and $k = 2$ at different times T using $N = 25 \times 25$ grid points and $dt = 0.01$

	$MQ - PS$	$(c = 0.37)$		$MQQI - PS$	$(c = 4.6)$	
T	L_∞	L_2	RMS	L_∞	L_2	RMS
1	9.99276×10^{-6}	4.48038×10^{-6}	2.52576×10^{-6}	1.15822×10^{-5}	5.21147×10^{-6}	2.93791×10^{-6}
2	6.77584×10^{-5}	2.52980×10^{-5}	1.42615×10^{-5}	7.47466×10^{-5}	3.1979×10^{-5}	1.80278×10^{-5}
3	2.78783×10^{-4}	7.76853×10^{-5}	4.37942×10^{-5}	2.54482×10^{-4}	1.0254×10^{-4}	5.78057×10^{-5}
4	5.77975×10^{-4}	1.50924×10^{-4}	8.50817×10^{-5}	5.74854×10^{-4}	1.47003×10^{-4}	8.28710×10^{-5}
5	5.72217×10^{-4}	1.24466×10^{-4}	7.01665×10^{-5}	7.96027×10^{-4}	1.64803×10^{-4}	9.29055×10^{-5}

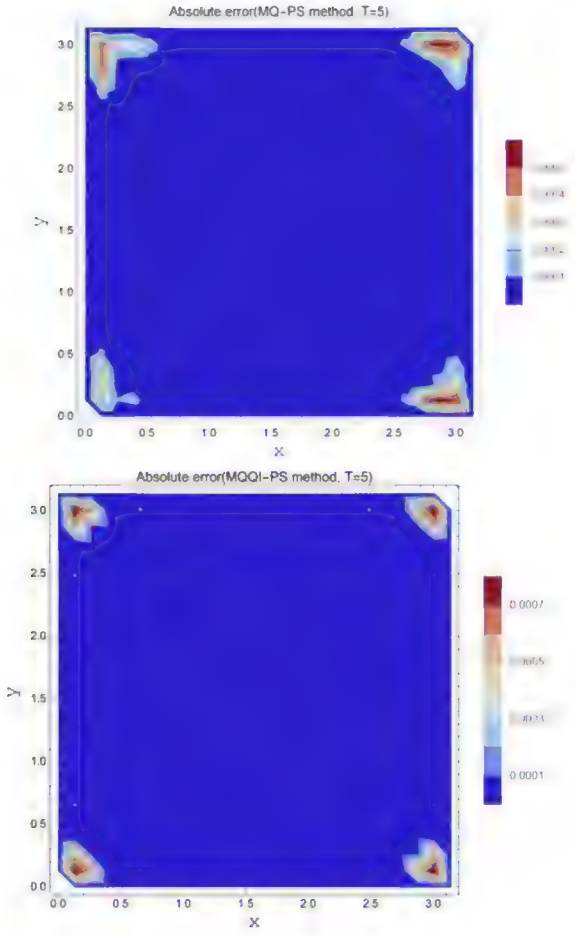

Figure 9: The contour plot of the absolute error norm for the MQ-PS method with MQ shape parameter $c = 0.37$ (up) and MQQI-PS method with MQQI shape parameter $c = 4.6$ (down) in Example 5 with $N = 25 \times 25$, $dt = 0.01$ at time t=5

$$u(x, 0) = u_0(x) \qquad x \in \Omega \subset \mathbb{R}^d (d = 1, 2), \tag{39}$$

Table 8: Error norms of Example 6 with $C = 0.5$ at different times T using $N = 121$ grid points, $dt = 0.001$, and MQQI shape parameter $c = 1.275$

T	L_∞	L_2	RMS	L_∞[43]	L_∞[9]
9	3.50847×10^{-4}	5.1875×10^{-4}	6.66931×10^{-5}	6.296×10^{-4}	4.518×10^{-1}
36	2.4275×10^{-4}	8.69372×10^{-4}	1.11771×10^{-4}	8.109×10^{-4}	2.293×10^{0}
1083.60803	$\times 10^{-4}$	1.5558×10^{-3}	2.00022×10^{-4}	2.568×10^{-3}	5.120×10^{0}

$$u_t(x,0) = v_0(x) \qquad x \in \Omega, \tag{40}$$

and Dirichlet boundary conditions

$$u(x,t) = g(t), \qquad t \in (0,T],\ x \in \partial\Omega. \tag{41}$$

We can transform problem (38) (41) into a system of coupled first order equations in time given by

$$\begin{cases} u_t(x,t) = v(x,t), \\ v_t(x,t) = -\alpha \triangle u - \sin(u), \end{cases} \tag{42}$$

with the initial conditions

$$u(x,0) = u_0(x) \qquad x \in \Omega \subset \mathbb{R}^d, \tag{43}$$

$$v(x,0) = v_0(x) \qquad x \in \Omega, \tag{44}$$

and boundary conditions

$$u(x,t) = g(t), \qquad t \in (0,T],\ x \in \partial\Omega. \tag{45}$$

The RBF-PS method described at the previous section is very efficient and can be applied to approximate solution of the system (42) (45). It is enough to replace the vector $\boldsymbol{U}^k$ in (30) by the vector $sin(\boldsymbol{U}^k)$. Numerical solutions obtained by this method are compared with the exact solutions and other existing methods.

Example 6. Consider problem (38) (41) with interval $x \in [-2, 58]$ and $\alpha = -1$.
The exact solution is given by:

$$u(x,t) = 4\tan^{-1}(\exp(\gamma(x - Ct) + \beta)), \tag{46}$$

where $\gamma = \frac{1}{\sqrt{1-C^2}}$.
The initial and boundary conditions are extracted from the exact solution easily.

Table 8 presents L_∞ errors, L_2 errors, and RMS errors in Example 6 with $C = 0.5$. The results are obtained by using $N = 121$ grid points, $dt = 0.001$, and the shape parameter $c = 1.275$. We compare our results with the reported

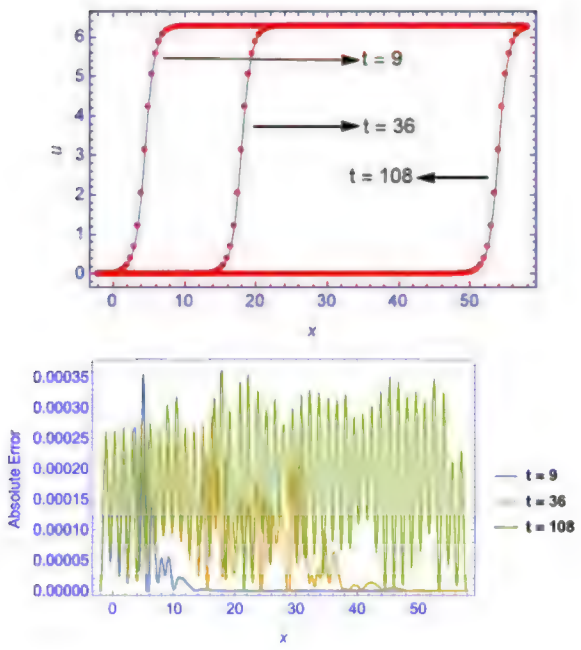

Figure 10: Numerical and exact solutions of Example 6 (up) and error of method (down) with $C = 0.5$, $N = 121$ and $dt = 0.001$

results in [43, 9]. As can be seen from the tables, the numerical results are in good agreement with the exact solution. Figure 10 represents numerical and exact solutions of Example 6 and error of method with $N = 121$, $dt = 0.001$ at different times T.

Example 7. In this example, we present numerical results of MQ-RBF-PS method for the two-dimensional sine-Gordon equation. Consider problem (38) (41) with domain $(x, y) \in [-7, 7] \times [-7, 7]$ and $\alpha = -1$.
The exact solution is given by [24]

$$u(x, y, t) = 4 \tan^{-1}(\exp((x + y - t))). \tag{47}$$

The initial and Dirichlet boundary conditions are extracted from the exact solution easily.

Table 9 presents L_∞ errors, L_2 errors, and RMS errors in Example 7. The results are obtained by using $N = 25 \times 25$ grid points, $dt = 0.001$, and the shape parameter $c = 0.31$. As can be seen from the tables, the numerical results are in good agreement with the exact solution. The graphs of the numerical and analytical solutions at $t = 5$ are shown in Figure 11. For Example 7, the contour plot of the absolute error norm of the MQ-PS method is portrayed in Figure 12. The MQ shape parameter c versus L_∞

Table 9: Error norms of Example 7 at different times T using $N = 25 \times 25$ grid points, $dt = 0.001$ and MQ shape parameter $c = 0.31$

T	L_∞	L_2	RMS
1	1.86749×10^{-3}	8.23484×10^{-4}	2.19909×10^{-4}
2	5.07197×10^{-3}	1.92593×10^{-3}	5.14315×10^{-4}
3	5.48379×10^{-3}	2.67973×10^{-3}	7.15615×10^{-4}
4	4.88027×10^{-3}	2.97766×10^{-3}	7.95177×10^{-4}
5	5.78486×10^{-3}	3.21738×10^{-3}	8.59192×10^{-4}

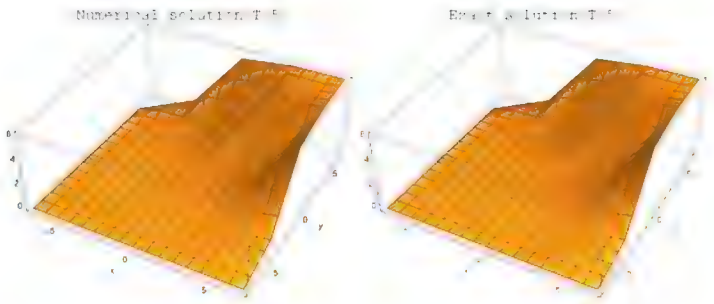

Figure 11: Numerical and exact solution of Example 7 with $N = 25 \times 25$, $dt = 0.001$ and MQ shape parameter $c = 0.31$ at time t=5

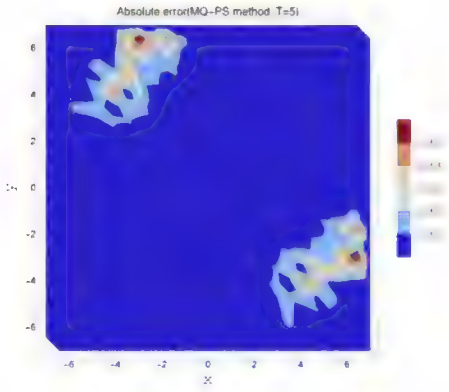

Figure 12: The contour plot of the absolute error norm of the MQ-PS method with $N = 25 \times 25$, $dt = 0.001$ and MQ shape parameter $c = 0.31$ at time t=5 for Example 7

corresponding to Example 7 is shown in Figure 13 when $t = 5$, $dt = 0.001$, and $N = 25 \times 25$.

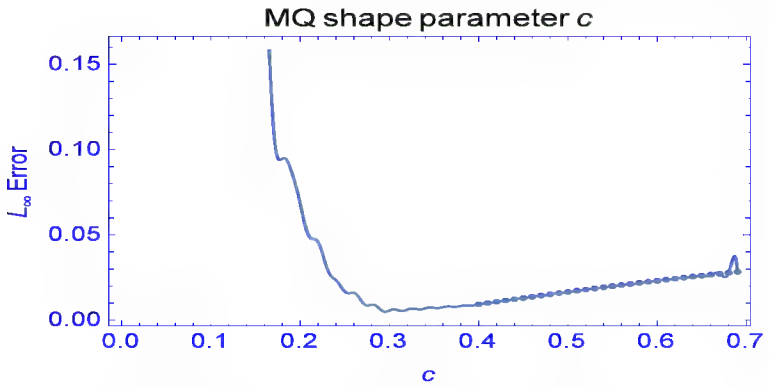

Figure 13: The plot of L_∞ error norm against MQ-Ps(c) with $N = 25 \times 25$, $dt = 0.001$ at time t=5 for Example 7

6 Conclusion

In this paper, a new radial basis function-pseudospectral (RBF-PS) method was proposed to solve the second order Klein Gordon equation with quadratic and cubic nonlinearity and sine-Gordon equation. In addition, a new technique was introduced to force approximations to satisfy the boundary conditions exactly each time. The proposed numerical method, which is truly meshless, was based on the MQ radial basis function, and MQ quasi-interpolation was used to compute RBF differentiation matrices to discretize the spatial derivative operators. The fourth-order Runge Kutta time stepping method was used to deal with the temporal part of the problem. Some illustrative examples have been given to show the accuracy and applicability of the presented method.

Acknowledgments

We thank the anonymous reviewers for helpful comments, which lead to definite improvement in the manuscript.

References

1. Abbasbandy, S., Azarnavid, B., Hashim, I. and Alsaedi, A. *Approximation of backward heat conduction problem using Gaussian radial basis functions*, Politehn. Univ. Bucharest Sci. Bull. Ser. A Appl. Math. Phys. 76 (2014),

67–76.

2. Abbasbandy, S., Ghehsareh, H.R. and Hashim, I. *Numerical analysis of a mathematical model for capillary formation in tumor angiogenesis using a meshfree method based on the radial basis function*, Eng. Anal. Bound. Elem. 36(12) (2012), 1811–1818.

3. Abbasbandy, S., Ghehsareh, H.R. and Hashim, I. *A meshfree method for the solution of two-dimensional cubic nonlinear Schrödinger equation*, Eng. Anal. Bound. Elem. 37(6) (2013), 885–898.

4. Ablowitz, M.J. and Clarkson, P.A. *Solitons, nonlinear evolution equations and inverse scattering*, Cambridge university press, 1991.

5. Azarnavid, B. and Parand, K. *Imposing various boundary conditions on radial basis functions*, arXiv:1611.07292, (2016).

6. Bahouri, H. and Shatah, J. *Decay estimates for the critical semilinear wave equation*, in Annales de l'IHP Analyse non linéaire, 1998.

7. Beatson, R.K. and Dyn, N. *Multiquadric B-splines*, J. Approx. Theory. 87(1) (1996), 1–24.

8. Beatson, R.K. and Powell, M.J. *Univariate multiquadric approximation: quasi-interpolation to scattered data*, Constructive approximation, 8(3) (1992), 275–288.

9. Bratsos, A.G. *A fourth order numerical scheme for the one-dimensional sine-Gordon equation*,Int. J. Comput. Math. 85(7) (2008), 1083–1095.

10. Chen, W., Fu, Z.-J. and Chen, C.-S. *Recent advances in radial basis function collocation methods*, Heidelberg: Springer, 2014.

11. Christiansen P.L. and Lomdahl P.S. *Numerical study of 2+1 dimensional sine-Gordon solitons*, Phys. D 2(3)(1981), 482–494.

12. Debnath, L. *Nonlinear Klein–Gordon and Sine-Gordon equations, in Nonlinear Partial Differential Equations for Scientists and Engineers*, Birkhäuser Boston, MA., 1997, 453–499.

13. Dehghan, M. and Shokri, A. *Numerical solution of the nonlinear Klein–Gordon equation using radial basis functions*, J. Comput. Appl. Math. 230(2) (2009), 400-410.

14. Drazin, P.G. and Johnson, R.S. *Solitons: an introduction*,Cambridge university press, Vol. 2, 1989.

15. Emamjome, M., Azarnavid, B. and Roohani Ghehsareh, H. *A reproducing kernel Hilbert space pseudospectral method for numerical investigation of a two-dimensional capillary formation model in tumor angiogenesis problem*, Neural Comput. Applic. (2017), 1–9.

16. Encinasa, A.H., Martín-Vaqueroa, J., Queiruga-Diosa, A. and Gayoso-Martínezb, V. *Efficient high-order finite difference methods for nonlinear Klein–Gordon equation*, I: Variants of the phi-four model and the form-I of the nonlinear Klein–Gordon equation, Nonlinear Anal. Model. Control, 20(2)(2015), 274–290.

17. Fasshauer, G.E. *RBF collocation methods as pseudospectral methods*,Boundary elements XXVII, 47–56, WIT Trans. Model. Simul., 39, WIT Press, Southampton, 2005.

18. Franke, R. *Scattered data interpolation: tests of some methods*, Math. Comp. 38(157) (1982), 181–200.

19. Gao, W. and Wu, Z. *Quasi-interpolation for linear functional data*, Journal of Computational and Applied Mathematics, 236(13) (2012), 3256–3264.

20. Gao, W. and Wu, Z. *A quasi-interpolation scheme for periodic data based on multiquadric trigonometric B-splines*, J. Comput. Appl. Math. 271 (2014), 20–30.

21. Gao, W. and Wu, Z. *Approximation orders and shape preserving properties of the multiquadric trigonometric B-spline quasi-interpolant*, Comput. Math. Appl. 69(7) (2015), 696–707.

22. Gao, W. and Wu, Z. *Solving time-dependent differential equations by multiquadric trigonometric quasi-interpolation*, Appl. Math. Comput. 253 (2015), 377–386.

23. Ghehsareh, H.R., Bateni, S.H. and Zaghian, A. *A meshfree method based on the radial basis functions for solution of two-dimensional fractional evolution equation*, Eng. Anal. Bound. Elem.61 (2015), 52–60.

24. Grella, G. and Marinaro, M. *Special solutions of the sine-Gordon equation in 2+ 1 dimensions*, Lettere al Nuovo Cimento. 23(12) (1978), 459–464.

25. Hardy, R.L. *Multiquadric equations of topography and other irregular surfaces*, Journal of geophysical research, 76(8) (1971), 1905–1915.

26. Hon, Y,.C. and Mao, X.Z. *An efficient numerical scheme for Burgers' equation*, Appl. Math. Comput. 95(1) (1998), 37–50.

27. Hosseini, V.R., Shivanian, E. and Chen, W. *Local integration of 2-D fractional telegraph equation via local radial point interpolation approximation*, Eur. Phys. J. Plus. 130(2) (2015), 33.

28. Kansa, E.J., Aldredge, R.C. and Ling, L. *Numerical simulation of two-dimensional combustion using mesh-free methods*, Eng. Anal. Bound. Elem. 33(7) (2009), 940–950.

29. Komech, A. and Komech, A. *Global attraction to solitary waves for Klein–Gordon equation with mean field interaction*, Ann. Inst. H. Poincaré Anal. Non Linéaire, 26 (2009), no. 3, 855–868.

30. Lin, J., Chen, W. and Chen, C.S. *A new scheme for the solution of reaction diffusion and wave propagation problems*, Appl. Math. Model. 38(23)(2014), 5651–5664.

31. Ling, L. *Multivariate quasi-interpolation schemes for dimension-splitting multiquadric* Appl. Math. Comput.161(1) (2005), 195–209.

32. Min Lu, X.,Ren Hong, W., and Chun Gang, Z.*Applying multiquadric quasi-interpolation to solve KdV equation*,J. Math. Res. Exposition 31(2) (2011), 191–201.

33. Myers, D.E., De Iaco, S., Posa, D. and De Cesare, L. *Space-time radial basis functions*, Comput. Math. Appl. 43(3) (2002), 539–549.

34. Parand, K., Abbasbandy, S., Kazem, S. and Rezaei, A.R.*Comparison between two common collocation approaches based on radial basis functions for the case of heat transfer equations arising in porous medium*, Commun. Nonlinear Sci. Numer. Simul. 16(3) (2011), 1396–407.

35. Powell, M.J.D. *Univariate multiquadric approximation: reproduction of linear polynomials*, Multivariate approximation and interpolation (Duisburg, 1989), 227–240, Internat. Ser. Numer. Math., 94, Birkhäuser, Basel, 1990.

36. Rostamy, D., Emamjome, M. and Abbasbandy, S. *A meshless technique based on the pseudospectral radial basis functions method for solving the two-dimensional hyperbolic telegraph equation*, Eur. Phys. J. Plus 132(6) (2017), 263.

37. Sarboland, M. and Aminataei, A. *Numerical solution of the nonlinear Klein–Gordon equation using multiquadric quasi-interpolation scheme*, Univ. J. Appl. Math. 3(3) (2015), 40–49.

38. Schaback, R. *Convergence of Unsymmetric Kernel-Based Meshless Collocation Methods*, SIAM J. Numer. Anal. 45(1) (2007), 333–351.

39. Shivanian, E. *Analysis of meshless local and spectral meshless radial point interpolation (MLRPI and SMRPI) on 3-D nonlinear wave equations*, Ocean Eng. 1(89) (2014), 173–188.

40. Shivanian, E. *A new spectral meshless radial point interpolation (SMRPI) method: a well-behaved alternative to the meshless weak forms*, Eng. Anal. Bound. Elem. 31(54)(2015), 1–2.

41. Shokri, A. and Habibirad, A. *A moving Kriging-based MLPG method for nonlinear Klein–Gordon equation* Math. Methods Appl. Sci. 39(18) (2016), 5381–5394.

42. Trefethen, L.N. *Spectral methods in MATLAB. Software, Environments, and Tools*, 10. Society for Industrial and Applied Mathematics (SIAM), Philadelphia, PA, 2000.

43. Uddin, M., Hussain, A., Sirajul, H.A. and Amjad A.L. *RBF meshless method of lines for the numerical solution of nonlinear sine-Gordon equation.* Walailak J. Sci. Tech. (WJST), 11(4) (2013), 349–360.

44. Wang, Q. and Cheng, D. *Numerical solution of damped nonlinear Klein–Gordon equations using variational method and finite element approach*, Appl. Math. Comput. 162(1) (2005), 381–401.

45. Wendland, H. *Scattered data approximation*, Cambridge university press, (17) 2004.

46. Wu, Z. and Schaback, R. *Shape preserving properties and convergence of univariate multiquadric quasi-interpolation*, Acta Math. Appl. Sinica (English Ser.) 10 (1994), 441–446.

47. Yin, F., Tian, T., Song, J. and Zhu, M. *Spectral methods using Legendre wavelets for nonlinear Klein\Sine-Gordon equations*, J. Comput. Appl. Math. 275 (2015), 321–334.

48. Zhang, Y., Liang, X.Z. and Li, Q. *A further research on the convergence of Wu-Schaback's multi-quadric quasi-interpolation*, J. Appl. Computat. Math. 2(4) (2013), 2–4.